Volume Transport Estimation of the Kuroshio Extension based on Subsurface Mooring Array and Satellite Altimetry

Haihong Guo[1,2], Zhaohui Chen[1,2*], Haiyuan Yang[1,2], Yu Long[3], Ruichen Zhu[1,2], Yueqi Zhang[1,2], Zhao Jing[1,2]

[1]Laoshan Laboratory, Qingdao, China.

[2]Frontier Science Center for Deep Ocean Multi-spheres and Earth System (FDOMES) and Physical Oceanography Laboratory, Ocean University of China, Qingdao, China.

[3]State Key Laboratory of Satellite Ocean Environment Dynamics, Second Institute of Oceanography, Ministry of Natural Resources, Hangzhou 310012, China.

Corresponding author: Zhaohui Chen (chenzhaohui@ouc.edu.cn)

Key Points:

- The vertical structure of the Kuroshio Extension is dominated by the barotropic and first baroclinic normal modes.
- The leading mode of Empirical Orthogonal Functions contains the first two vertical normal modes.
- The Kuroshio Extension transport can be well reproduced by surface geostrophic flow and hydrographic data.

Abstract

The vertical structure of the Kuroshio Extension (KE) is investigated using velocity measurements from a subsurface mooring array. Mode decomposition based on climatological Temperature/Salinity (T/S) data shows that the barotropic and first baroclinic normal modes dominate the vertical structure of the zonal flow in the KE. This structure is also well described by the leading mode of Empirical Orthogonal Functions (EOFs) that contains the first two vertical normal modes. Further analysis demonstrates that the projection coefficient of the mooring velocity onto the summed vertical mode could be well represented by the surface geostrophic velocity. Therefore, we propose a dynamic method that relates the surface geostrophic flow and the vertical structure of the zonal flow. The applicability of this method is verified with both reanalysis datasets and estimation from hydrographic data. The findings implicate that the KE transport can be well reproduced by surface geostrophic flow and climatological T/S data only.

Plain Language Summary

The Kuroshio Extension (KE) plays an important role in the mid-latitude North Pacific climate system. To better understand the KE dynamic and its influences, it is very important to estimate the KE transport. However, direct observation is very difficult in this area. Combining a subsurface mooring array and satellite altimetry, the vertical scale of the KE is explored in this study using mode decomposition methods. The vertical structure of the KE is dominated by the barotropic and first baroclinic modes. The relationship between the vertical structure of the zonal velocity and surface geostrophic flow in the KE region is further investigated. Based on this relationship, the KE transport can be well estimated by surface geostrophic flow and hydrographic data.

1 Introduction

The Kuroshio Current (KC), which originates from the Philippines coast and leaves the Japanese archipelago in the midlatitude ocean, acts as a mass, momentum, and heat conveyor connecting the tropical and extratropical Northern Pacific Ocean. After leaving the western boundary, the Kuroshio veers eastward as a zonal flow, i.e., the Kuroshio Extension (KE) jet. This eastward jet builds a sharp potential vorticity front and a temperature front in the mid-latitude North Pacific, resulting in abundant shedding of eddies through baroclinic/barotropic instability (Hurlburt et al., 1996). These eddies draw (return) energy from (to) the mean flow in the upstream (downstream) KE (Yang et al., 2017). In addition to rich oceanic processes, the KE has also been regarded as an important region of coupled ocean-atmosphere activities (O'Reilly and Czaja, 2014). Qiu (2003) showed that the KE is remotely forced by wind stress curl anomalies related to the Pacific Decadal Oscillation (PDO). Besides, the feedback between ocean mesoscale eddies and the atmosphere is fundamental to the dynamics of the KE jet (Ma et al., 2015).

The KE plays an important role in modulating the environmental features from the surface to the deep layer (Bishop et al., 2012; Yang et al., 2021). In the surface layer, as a typical subtropical western boundary extension, the KE is a hot spot of high marine heat wave intensity with large sea surface temperature variability (Oliver et al., 2021). In the lower layer, the KE is a critical source of the North Pacific intermediate water (NPIW), characterized by a vertical salinity minimum (Hiroe et al., 2002), which is important for the carbon cycle between subarctic

and subtropic (Tsunogai et al., 2002). Besides, the deep convection that occurs in the KE region forms vertically homogeneous water, the Subtropical Mode Water (STMW). The STMW is carried away from its formation area and widely distributed (Suga and Hanawa, 1995). In the deep layer, evidence was found that the abyssal currents are weakly bottom intensified (Bishop et al., 2012). Therefore, in the KE region, abundant multi-scale oceanic processes and air-sea interactions play an essential role in the extratropical North Pacific climate system (Jayne et al., 2009; Kida et al., 2015; Ma et al., 2015; Qiu et al., 2007;). However, the vertical scale of the KE remains poorly understood and requires more observational evidence.

Moreover, to better understand the role of the Kuroshio in the climate system, it is necessary to first reveal the mass/heat transport meridionally and zonally. Along the Kuroshio pathway, there have long been numerous hydrographic and current observations in the past decades near the Philippines coast, east of Taiwan island, the Eastern China Sea (ECS) shelf break, south of Japan. However, in the KE region, directly observed transport for the Kuroshio in this region has been lacking due to the complex structure, strong currents, and rich eddies, which pose a serious challenge for in-situ observation. Despite these difficulties, there have been several types of observations that have captured the KE transport. Using the hydrographic data occupied across the Kuroshio extension along the longitudes of 165°E, Joyce (1987) provided an estimation of the eastward KE transport (56 ± 2 Sv). Based on a current meter mooring, Hall (1989) more directly measured the transport of the KE with a value of 87 ± 21 Sv. Furthermore, Yoshikawa et al. (2004) calculated transport of 163 Sv across 146°25'E and 113 Sv across 152°30'E using Lowered ADCP data. More systematical observations from the Kuroshio Extension System Study (KESS) project were used to estimate a total downstream transport of 114 ± 13 Sv and a weaker Eulerian averaging transport of 79 Sv for the KE (Jayne et al., 2009). Except for direct observation, the surface transport of the KE is linearly related to the SSH difference across the KE (Qiu 2003), which provided a reasonable proxy of the KE strength. However, it is easy to note that these estimations are quite different in time and space. Given the insufficient observations in this area, the biases between different observations are hard to reduce, not to mention the long-term volume transport. To better understand the role of the KE in modulating the ocean and atmosphere, it is necessary to quantify the volume transport of the KE as well as the vertical structure.

There have been several projects and sections that provided a valuable estimation of the KE transport. For example, the KESS project employed inverted echo sounders with bottom pressure gauges and current meters (C-PIES), subsurface moorings, Kuroshio Extension Observatory (KEO) surface buoy, and dozens of Argo profiling floats, which could provide a good estimation for the KE. In the SubArctic Gyre Experiment (SAGE), intensive observations were conducted in the KE region with ADCPs/CTDs (Yasuda 2004), which provide an estimation of the volume transport in the intermediate layer (Talley et al., 1995; Hiroe et al., 2002). However, the long-term variabilities of the total KE transport remain unclear. Therefore, longer observations are needed to provide a comprehensive view of the complex circulation in the KE region. Since 2015, China has initiated the Kuroshio Extension Mooring System (KEMS, https://cn-kems.net/) with an array of subsurface moorings across the KE. (Figure 1, detailed information is provided in the following section). The advantage of a subsurface mooring array is that it can provide a direct long-term observation and cover the full velocity of the upper and some deep flow information.

It is noteworthy that limited subsurface moorings are sparsely deployed in the KEMS array with over 200 km between each mooring, which makes it hard to directly calculate the KE

transport. The main purpose of this paper is to explore the dynamic relationship between the vertical structure of the observed velocity and the surface geostrophic flow by combing the climatology hydrographic and altimetry data. Then, an estimation method of volume transport is extended to calculate the KE transport based on this dynamic relationship. The paper is organized as follows: Data and methods are first described in Section 2, followed by presenting the results of the vertical structure, its connections with the geostrophic flow, and the volume transport estimation in section 3. Finally, in section 4, we will summarize the results.

2 Data and method

2.1 KEMS Mooring Data

As part of the KEMS project, five subsurface moorings were successively deployed along a line crossing the axis of the KE since 2015. Following the last cruise in July 2022, there are now five subsurface moorings (M1, M2, M3, M4, and M5), which range from 32.4°N, 146.2°E to 41.0°N, 151.2°E. The KE jet crosses over the mooring array (Figure 1a) with the M3 mooring being located at the axis. It should be noted that M5 is far away from the axis of the KE jet, which is not used in this study. In 2015, M1 was deployed at a water depth of ~5600 m with two ADCPs (RDI Workhorse Long Ranger 75 kHz), four CTDs (SBE 37-SM), three Aquadopp-DW/SeaguardRCM current meters, and a chain of SeaBird56 temperature loggers equipped (Figure 1b). Until the last recovery, the longest-running mooring, M1, had been maintained for almost 7 years, and even the shortest-running mooring used in this study (M4) had been maintained for more than 2 years. Therefore, these moorings could provide in situ current and temperature/practical salinity (T/S) data in the upper 1500 m ocean.

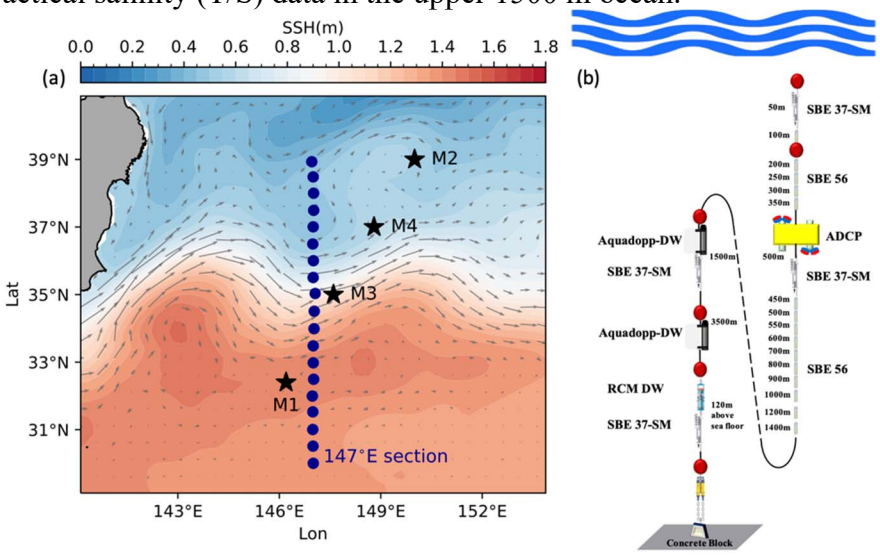

Figure 1 (a) Locations of KEMS subsurface moorings (black stars) from November 2015 to July 2022. The blue dots denote a historical hydrographic section (147°E) used for comparison in this study. The color shading and gray arrows represent the climatological sea surface height (SSH) and the surface geostrophic current. (b) Schematic of the design of the moorings.

The velocity data used in this study is mainly obtained by the ADCPs, which were deployed at around 500-m depth, with one looking upward and the other downward, which could roughly cover the upper 1000 m. Their sampling interval and vertical bin size were set to 1 hour and 16 m, respectively. The ADCPs records were interpolated vertically onto a standard depth of 10 m

intervals. Moreover, three current meters (CM) were deployed at 1500, 3500, and 5500 m after 2016. The sampling intervals of the temperature chain, CTDs, and current meters are 1, 5, and 30 min, respectively. All instrumental data were filtered with a cutoff period of 2 days (the local inertial period is ~22 h) to remove the tidal effect and other high-frequency motions such as inertial gravity waves.

2.2 Other Datasets

Since the moorings are located relatively far away from each other, the KE could not be well covered. More datasets are needed to establish and examine the dynamic mechanism. Therefore, the gridded daily altimeter data with a spatial resolution of 1/4° from Archiving, Validation, and Interpretation of Satellite Data in Oceanography (AVISO) (https://www.aviso.altimetry.fr/) is used to provide the absolute surface geostrophic current (Ducet et al., 2000). The AVISO dataset started in 1993 and has been updated to the present. To explore the vertical structure of the KE, the monthly climatological World Ocean Atlas (WOA18) temperature and salinity (Locarnini et al., 2018; Zweng et al., 2019) were used to perform vertical mode decomposition analysis. The stratification used for the decomposition is calculated by using the WOA 18 T/S data within a 0.5°-radius circle centered at the mooring site where the monthly climatological data is interpolated into the daily field. It should be noted that the WOA18 only provides monthly climatological T/S profiles in the upper 1500 m. Therefore, the profiles below 1500 m are replaced by climatological means. We also use the eddy-resolving simulations of the Oceanic General Circulation Model for the Earth Simulator (OFES) to further validate the dynamic mechanism between surface geostrophic flow and vertical structure of the horizontal velocities (Masumoto et al., 2004). The OFES was spun up for 50 years and integrated forward from 1950 using daily surface forcing of the National Centers for Environmental Prediction/National Center for Atmospheric Research (NCEP/NCAR) reanalysis product (Kalnay et al., 1996). In this study, we only used the OFES data after 1993 to match the same period with the AVISO data for comparison. The absolute geostrophic velocities derived from the WOA18 represent the monthly climatological background flow. To test the applicability of this method, absolute geostrophic velocity data based on hydrographic data at the 147°E line is used for comparison (Long et al., 2018; Long et al., 2019).

2.3 Vertical Normal Mode Decomposition

To investigate the vertical structure of the KE, we first employed vertical normal mode decomposition for the horizontal velocity. In the linearized hydrostatic equations, the vertical components of the horizontal velocity (*u, v*) and the pressure field (*p*) in terms of an eigenfunction can be projected onto complete orthogonal bases (Vallis, 2017) that satisfies:

$$\frac{d}{dz}\left(\frac{1}{N^2}\frac{dC_n(z)}{dz}\right)+\frac{1}{c_n^2}C_n(z)=0, \tag{1a}$$

$$\frac{d}{dz}C_n(0)=-\frac{d}{dz}C_n(-H)=0, \tag{1b}$$

where C_n are the orthogonal basses, c_n are the eigen speeds, and N is the buoyancy frequency associated with the mean background stratification. The projected intensity of each normalized baroclinic mode on the horizontal velocity $v(z,t)$ is determined by

$$P_{nv}(t)=\frac{\int_H^0 v(z,t)C_n(z)dz}{\int_H^0 C_n^2(z)dz}, \tag{2a}$$

$$v_n(z,t) = C_n(z)P_n(t), \quad (2b)$$

where $P_n(t)$ is the projection coefficient of the zonal velocity, representing how strongly the observed velocity projected onto each mode, and $v_n(z,t)$ is the velocity anomaly of the *n*th baroclinic mode (Ma et al., 2022). The explained contribution of each mode can be calculated by the variance ratio between the mode velocity and full velocity.

2.4 The EOF Decomposition

Empirical Orthogonal Functions (EOFs) were also used to extract the dominant vertical structure of the observed full-depth zonal velocity. The climatologic mean of the moored velocity at each depth was removed before EOF decomposition. It should be noted that the EOF decomposition does not require additional hydrostatic information (T/S) like the vertical mode decomposition. Therefore, it could not provide a distinct decomposition with different normal modes like the vertical normal mode. However, the main EOF mode usually contains a mixing of different vertical normal modes (Ren et al., 2018). The benefit of EOF decomposition is that it could explain larger variance in a single mode, which makes it easier to connect the principal component (PC) series with the surface geostrophic flow. However, EOF decomposition is a purely statistical method that first requires the local velocity and is hence impossible to achieve the decomposition except for the mooring position. Therefore, it is instructive to combine these two methods and take their individual advantages.

3 Results

In this section, we first employ the vertical mode and EOF decompositions for the zonal velocity of M1 in sections 3.1 and 3.2. To explore the relationship between these two methods, a mixed vertical normal mode was deduced to connect these two vertical modes in section 3.3. Then we extended it to other mooring sites in section 3.4. The dynamic relationship is further verified by using the OFES dataset in section 3.5. Section 3.6 presents the KE transport estimation based on vertical modes.

3.1 Vertical Normal Modes

The southernmost site, M1, was discussed in this part. Before exploring the vertical modes and their variability, it is necessary to provide an overview of the full velocities. Figure 2a shows the depth-time plots of the observed daily mean zonal velocity at the M1 site. The zonal flow at this site is mainly located in the upper 1500 m, where a maximum daily mean velocity of up to 0.98 m/s is observed near the surface. To better elucidate the vertical structure, we apply the vertical normal mode decomposition at this site (Equation 1) based on WOA18. The mooring temperature chain was also used in the decomposition, whose vertical mode is very similar to the WOA18 data. Besides, in order to extend this method into other regions, it is better to keep using WOA18 data and validate its adaptability. Then, we project the zonal velocity onto vertical modes to compare it with the surface geostrophic flow by using Equation 2.

The mode decomposition shows that the vertical structure of the horizontal velocity is dominated by the barotropic mode and the first baroclinic mode. The barotropic mode was normalized to 1 (not shown), which could explain 25% of the total variance. The first baroclinic mode is significantly surface-intensified with a zero crossing at 1500 m, which explains 57% variance for the zonal velocity above the zero crossing (Figure 2b). Therefore, the first two

modes could explain over 80% variance (Table 1), and dominate the main variability of the zonal velocity at M1. We sum up these two modes to reproduce the zonal velocities. The summation could well reproduce the zonal velocity, including the strength, variability, and vertical structure (Figure 2a, c). It is noteworthy that the reproduced velocity is not exactly consistent with the geostrophic flow during some periods (February 2020 and May 2020). A more detailed check shows that these differences are due to nonlocal eddies originating away from the mooring (Supplementary Figure 1). These eddies could trap fluid parcels and come from other regions (Zhang et al., 2014), which will bring remote T/S signals and break the local mode decomposition. Nevertheless, the reproduced velocity correlates well with the moored velocity with correlations ranging from 0.79 to 0.99 at different depths. The correlation slightly decreases as depth increases, where a minimum occurs at around the depth of zero-crossing, but it still reaches 0.79. We can confidently suggest that these two modes dominate the variability of velocity at M1.

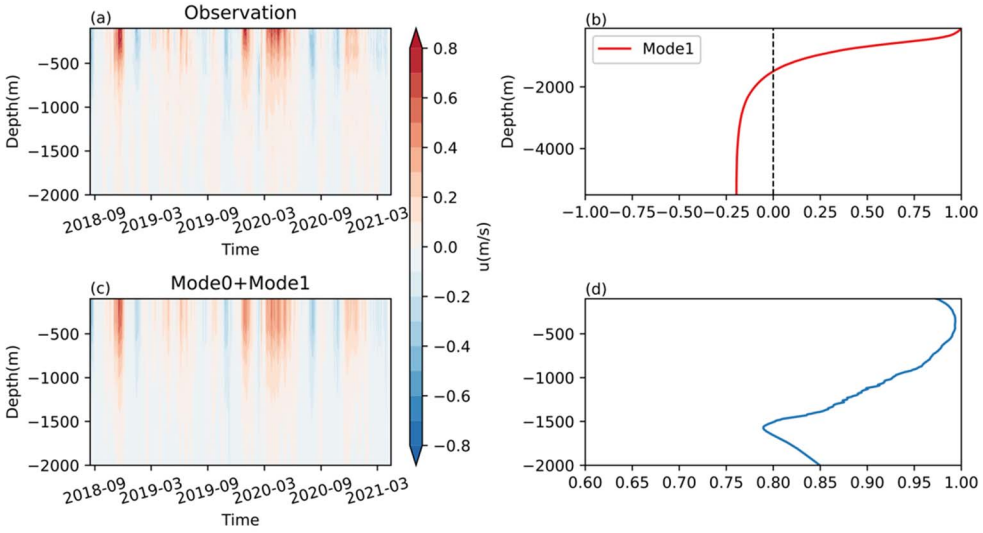

Figure 2 (a) The observed zonal velocity at the M1 site. (b) The vertical structure of the first baroclinic mode. (c) Reconstructed zonal velocity based on the sum of zonal velocity projected onto barotropic and first baroclinic modes. (d) The correlation between observed velocity and reconstructed velocity at each depth.

3.2 EOF Modes

To better understand the vertical structure of the horizontal velocity and how the different vertical modes mix, we use EOF analysis to further decompose the complex variability patterns. It is found that the dominant EOF mode tends to mix different vertical normal modes (Ren et al., 2018), where a direct connection between the AVISO geostrophic velocity and mooring velocity should be easier to establish. Figure 3 shows the mode-1 EOF (EOF1) of the zonal velocity at M1 and its principal component (PC1). The EOF1 could explain 92% of the total variance of mooring velocity, which is similar to the variance contribution of the first two vertical normal modes (Table 1). The correlation between the PC1 of zonal velocity and AVISO geostrophic velocity reaches 0.87.

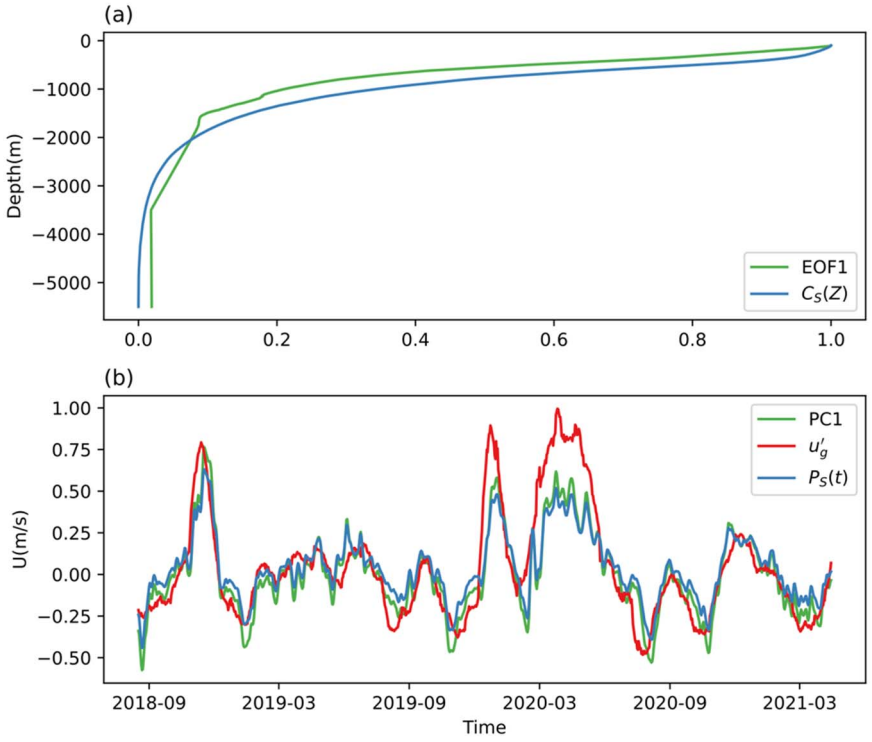

Figure 3 (a) The vertical structure of the EOF1 (green) and summed barotropic and first baroclinic normal mode (blue) at the M1 site. (b) The projection coefficients of the moored zonal velocity onto EOF1 (green) and the summed vertical normal mode (blue), and the time series of the surface zonal geostrophic velocity at the M1 site (red).

The explained variance shows that the EOF1 contains a mix of barotropic and first baroclinic modes in the KE region. This is not surprising, since EOF analysis is a purely statistical method without further dynamic information. The vertical normal mode could provide detailed information by considering the hydrostatic data and obtaining diverse modes. Therefore, unlike the EOF mode with orthogonality, the vertical normal mode is also constrained by the vertical boundary condition, which results in diverse modes. For example, the EOF1 mode captures in-phase variability of the zonal velocity, while the barotropic mode requires not only in-phase but also uniform distribution in depth. However, each vertical normal mode corresponds to an independent time series ($P_n(t)$ in Equation 2a), which is hard to compare with the AVISO geostrophic flow. The EOF decomposition could reproduce the main feature of zonal velocity by using a single mode but highly depends on the in-situ observation, which makes it impossible to predict the structure of the KE other than the mooring site. Therefore, we will explore the connection between these two mode decomposition methods in the next section.

3.3 Mixed Vertical Modes

Before investigating the connection between the two mode decomposition methods, it is useful to consider their similarities and differences. Both the first baroclinic mode and the EOF mode are surface intensified (Figure 2b, 3a). However, the sign of the velocity of the first baroclinic mode reverses in the deep ocean, while the EOF1 mode just decays as depth increases. Given that the strength of the full velocity in the deep layer is much weaker than the upper layer, and the higher baroclinic modes make a little contribution, the reversed flow of the first baroclinic mode could be treated as a balance of the barotropic mode in the deep ocean. The

mode decomposition also shows that the first baroclinic mode is in the same direction as the barotropic mode (uniformly identical to 1, not shown) in the upper layer and reverses in the deep layer (Figure 2b). Therefore, the barotropic component tends to strengthen the upper layer flow and cancel the deep layer flow of the first baroclinic component. It is well known that the first baroclinic mode dominates the vertical structure in the world ocean (Chelton et al., 1998). However, in the KE region, using this single mode will underestimate the full velocity, since the barotropic mode could explain 25% variance and is non-negligible. Therefore, it is necessary to consider both the barotropic and first baroclinic modes in reconstructing of the full velocity.

The connection between the two vertical normal modes can also be understood from the time variability. First, the correlation of the time series between the barotropic mode and the first baroclinic mode is 0.77. Moreover, the ratio between the time series amplitude of the barotropic mode ($P_0(t)$) and the first baroclinic mode ($P_1(t)$) is 0.21, while the strength ratio between these two modes in the deepest layer ($r_c = |C_1(H)|/|C_0(H)|$) is 0.196. Therefore, it is reasonable to infer that the barotropic mode and first baroclinic mode neutralize each other at the bottom. Since the barotropic mode is depth independent, we could linearly add it up with the first baroclinic mode by taking a weight of r_c,

$$C_s(z) = C_1(z) + r_C C_0(z). \quad (3)$$

As a result, we obtain a summed mode ($C_s(z)$) combining the first two vertical normal modes, which is similar to the EOF1. To better understand the relationship between the dominant EOF1 and the summed vertical modes ($C_s(z)$), we have normalized these two modes ($C_s(z)$ and EOF1) to 1 at the surface before further analysis. Figure 3a shows the profile of these two modes, whose vertical structures are nearly identical. It should be noted that the EOF1 only uses the observed velocity, while the summed vertical normal mode, on the contrary, only uses the hydrostatic data. Despite different methods, the consistency between the two modes (Figure 3a, b) indicates both the EOF decomposition and the vertical mode decomposition can well capture the main vertical structure.

To investigate the strength of the observed velocity projected onto the main mode of the two methods, we further calculate the projection coefficients using Equation (2a). The projection coefficients of the two modes are nearly identical, which further demonstrates their consistency (Figure 3b). Therefore, the PC1 could be well reproduced by linearly combing the barotropic and first baroclinic vertical normal modes ($P_s(t)$). Both these two main vertical modes are normalized to 1 at the surface, therefore, the projection coefficients (PC1 and $P_s(t)$) represent the strength of the surface flow. For the oceanic currents, if we focus on low-frequency and large-scale movement, these currents can be treated as geostrophic flows. The surface geostrophic flow could be easily derived from AVISO altimetry data. Figure 3b shows the time series of AVISO geostrophic flow anomaly (u'_g), the PC1, and the $P_s(t)$. Since the EOF decomposition has removed the statistical mean, we also calculated the anomaly of the geostrophic flow to focus on the time variability. The correlations between u'_a and the time series of the two modes are 0.86 ($P_s(t)$) and 0.87 (PC1). These consistencies show that the surface geostrophic flow anomaly could be well treated as an approximation of the projection coefficients.

3.4 Other Mooring Sites

To estimate the KE transport, it is necessary to extend this relationship to other mooring sites. Following the analysis at the M1, we also conducted two types of mode decomposition for other moorings. The zero crossing of the first baroclinic mode deepens at high latitude, with values of 1500 m (M1), 1630 m (M3), 1750 m (M4), and 1800 m (M2). This is easy to

understand since the temperature in the upper layer drops as latitude increases, which results in a weak stratification and a large vertical scale of the upper layer ocean. Consequently, the flow at a high latitude becomes more barotropic and the ratio between the strength of barotropic and first baroclinic modes (r_c) also increases as the latitude increases (Table 1). Although the vertical structures slightly vary at different sites, the observed horizontal velocity could also be well reproduced by the first two modes, which explains over 80% variance for other sites (Table 1). The explained variance of EOF1 is slightly larger than the vertical normal modes. That's not surprising because the EOF1 may contain higher baroclinic modes, which results in a tiny difference (Figure 3a). However, the explained variance of these higher baroclinic modes is relatively small, so we can neglect them.

Table 1 The ratio between the strength of the barotropic and first baroclinic modes, the explained variance of the summed vertical mode and EOF1 mode, and the correlations between the AVISO geostrophic velocity and these two modes (PC1 and $P_s(t)$) for all sites.

	M1 (32.4°N)	M3(35°N)	M4(37°N)	M2(39°N)
r_c	0.196	0.200	0.231	0.259
Var ($C_s(z)$)	82%	82%	88%	85%
Var (PC1)	92%	90%	89%	88%
Cor (u_g', $P_s(t)$)	0.86	0.83	0.72	0.83
Cor (u_g', PC1)	0.87	0.84	0.73	0.83

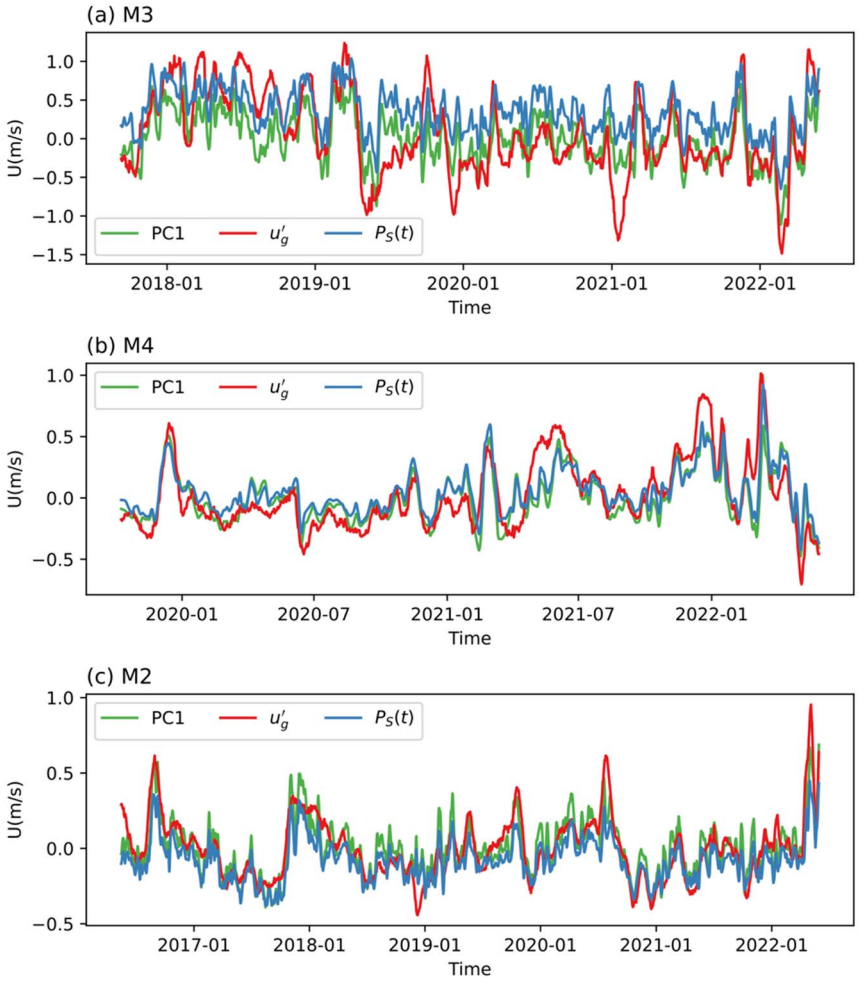

Figure 4 Same as Figure 3b but for the M3 (a), M4 (b), and M2 (c) sites.

For other moorings, the explained variance of the two modes demonstrated the same dynamical relationship as M1. Besides, the projection coefficients further confirm this relationship, where the similarity between geostrophic flow anomaly (u'_g), the PC1, and the $P_s(t)$ can hold for all other sites (Figure 4). The correlations between u'_g and the mode projection coefficient are over 0.8 for M1, M2, and M3 (Table 1). Although the correlations at M4 are slightly smaller than other moorings, which may be due to a short observation period of 2 years, they are still over 0.7. Therefore, for other sites, the projection coefficients of these two modes (PC1 and $P_s(t)$) could also be represented by the geostrophic flow. Based on this relationship, the vertical profile of the zonal velocity could be reproduced by combining the AVISO geostrophic flow and the WOA hydrotropic data, which provides a new method to estimate the KE transport.

3.5 Vertical Structure of KE in OFES

Combining two mode decomposition methods suggests a dynamic relationship between the vertical structure of the zonal velocity and the altimetry observed geostrophic current, but four moorings are too sparse to sufficiently cover the KE jet. To examine if this relationship can hold in the entire KE region, we extend this method to the OFES dataset. We first applied this method

at the same position as the M1 site in the OFES. Figure 4 shows the EOF1, the summed vertical mode, and the projection coefficients of these two modes. Both the vertical structure and the variability exhibit high similarity between EOF and summed vertical mode. Since we could use the time-dependent hydrographic data in OFES to calculate the stratification, we could eliminate the effect of eddies coming from other regions. Not surprisingly, the performance of mode decomposition in the OFES simulation is much better than the observed results based on the WOA18 data. It is interesting to note that there still exist some strong peaks, where the geostrophic current and the projection coefficient show an obvious difference. This is not surprising, since for strong eddy the nonlinearity and centrifugal force (Zhu et al., 2020) cannot be ignored, which will break the geostrophic balance. The results at other sites are essentially the same as the M1 (not shown), which implies that this dynamic relationship also holds at other sites in the OFES data.

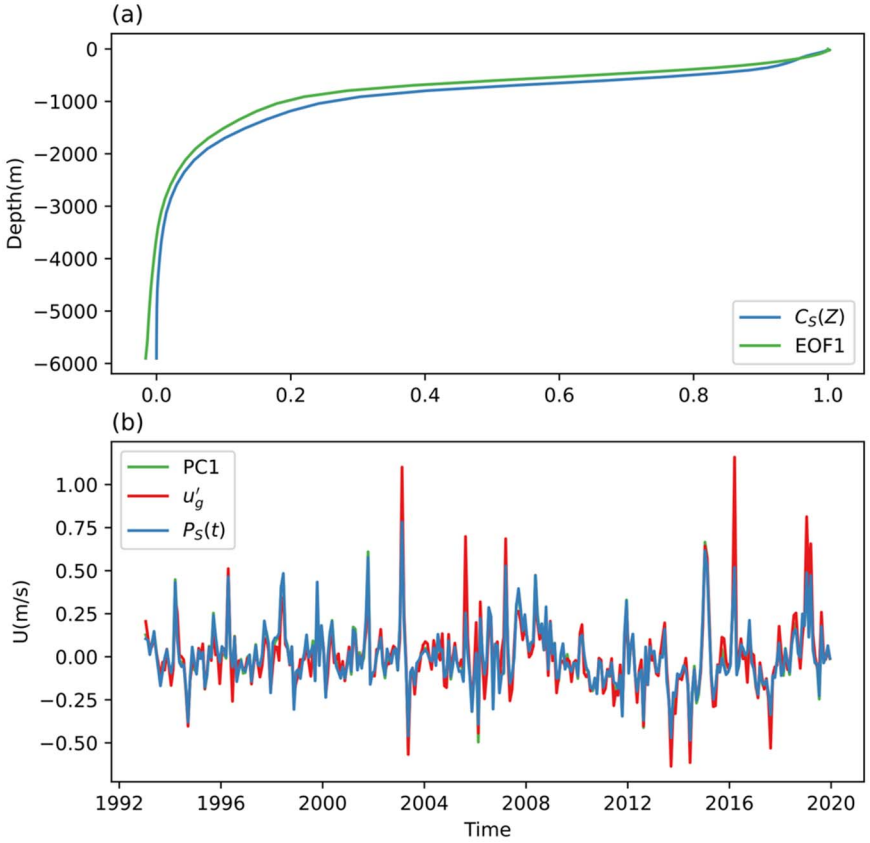

Figure 5 Same as Figure 3 but for the OFES dataset.

To further test the ability of the mode decomposition methods to reproduce the KE transport, it is necessary to extend this method to the entire KE region. The OFES could provide full-depth velocity as well as the surface geostrophic flow, which is helpful to directly calculate the transport and estimate the transport base on mode decomposition. Since the line between the M1 and M4 sites could well cover the KE jet (Figure 1), we first reproduced the vertical profile of the horizontal velocity by using the hydrostatic data and the modeled sea surface height along the mooring track from M1 to M4. It should be noted that the summed vertical modes and the EOF mode represent the variability without the statistical mean (Figure 4). Therefore, the climatologic velocities were added to the reconstructed velocities. Then we calculated the cross-sectional transport based on the reconstructed velocity and the velocity directly derived from the

model, respectively. Figure 6 shows these two types of transport from 1993 to 2019. The consistency between these two types of transport shows that the mode reconstruction method could reproduce cross-sectional transport well, including its strength and variability (Figure 6). The averaged transport directly calculated from the modeled velocities is 58.3+11.9 Sv, while the averaged reconstructed transport is 54.7+14.4 Sv. As for the variability, the correlation between the modeled transport and the reconstructed transport is 0.88. We can confidently conclude that the dominant features of the barotropic and first baroclinic modes hold in the entire KE region, which can support the estimation of the KE transport.

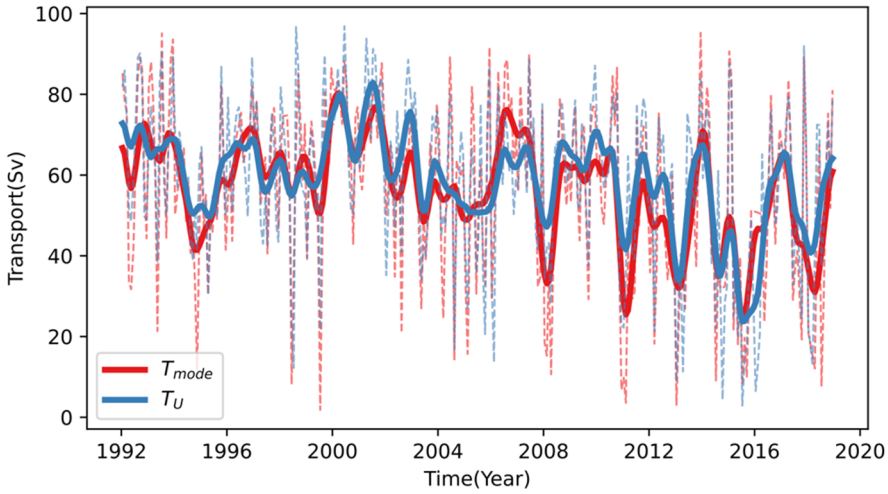

Figure 6 The cross-sectional transport from M1 to M2 using the OFES modeled velocity (blue) and reconstructed velocity (red), respectively. The dashed lines denote the monthly mean transport and the solid lines denote the low-pass filtered transport with a 13 months cutoff.

3.6 Estimated KE Transport

Next, we apply this method in the real ocean to estimate the KE transport by combining the AVISO geostrophic velocity and the WOA T/S data. Since the mode estimation method was based on the geostrophic balance and may be affected by high-frequency variability when there were strong currents, we use the monthly mean geostrophic flow from the AVISO datasets. The monthly climatological WOA T/S data are used to compute the vertical normal mode and background geostrophic velocity.

Before further comparison, it is noteworthy that the relationship between vertical normal mode and EOF mode will lose its adaptability near the coastal region, where the Kuroshio current could extend to the bottom. In this case, the bottom current is not weaker than the upper layer flow, which will make it impossible to linearly sum up the barotropic and first baroclinic modes. Therefore, we chose some historical sections away from the Japanese coast for comparison. We first provide a comparison of the KE transport along the 147°E line with observation based on absolute geostrophic velocity (Long et al., 2019). Absolute geostrophic velocity along the 147°E line was obtained from hydrographic data. The averaged cross-section transport from 30°N to 40°N at this section is 48.2±9.0 Sv based on the inverse method, while the mode reconstructed transport (57.2+11.3 Sv) is slightly stronger than observation. Despite this difference, the time variability of the KE transport is quite similar to the mode estimation. As shown in Figure 7, the observation is highly correlated with the mode estimation with a correlation reaching 0.81.

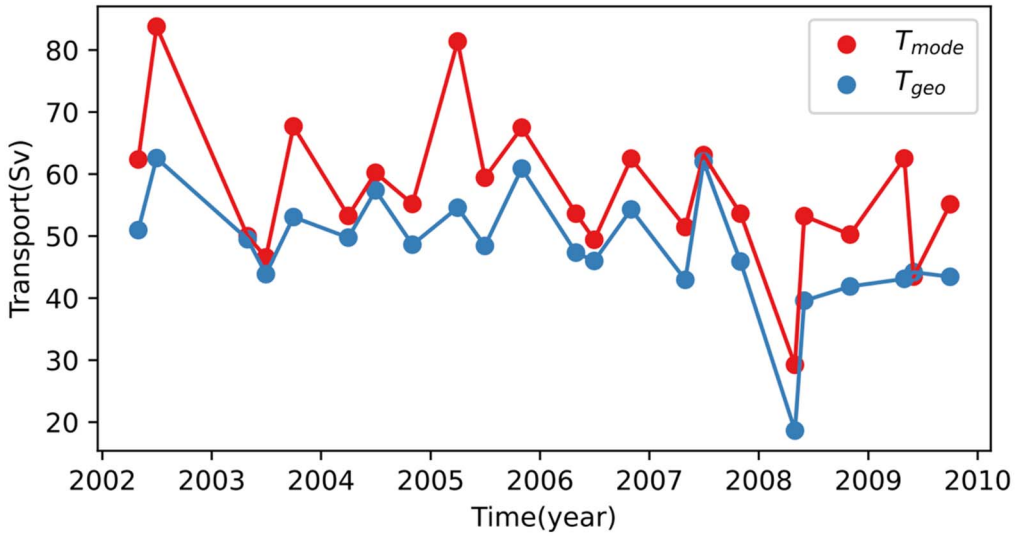

Figure 7 The volume transport across the 147°E line based on the hydrographic data (blue) and the mode reconstruction (red).

Besides, Jayne et al. (2009) used combined observations from the KESS to estimate the strength and structure of the KE and its recirculation. Based on the Eulerian average, they gave an estimate of 79 Sv for the KE transport. The mode estimation method suggests an average transport of 85 Sv for the KE over the same period and the same location as the KESS, which is quite similar to its estimation. Based on Lowered ADCP data, Yoshikawa et al. (2004) showed that the eastward Kuroshio Extension transport was 163 Sv across 146°25'E in May 2001 and 113 Sv across 152°30'E in July 2000. However, the mode estimation method gives 97 and 94 Sv in these two sections, which is weaker than the Lowered ADCP estimation. This reduction may be due to the smoothing effect using the monthly mean altimeter data, while the ADCP observation may contain non-geostrophic components.

4 Summary and Discussion

In this study, we have investigated the vertical structure of the zonal velocity in the Kuroshio Extension region using a mooring array. The vertical structure of the zonal velocity is dominated by the barotropic and first baroclinic modes, which explain over 80% variance for all mooring sites. This structure is also well reproduced by EOF decomposition, where the EOF1 contains mixed signals from these two modes. By connecting the vertical normal modes and EOF1 mode, a new transport estimation method is proposed to estimate the Kuroshio Extension transport.

The first baroclinic mode contributes most to the full velocity in all sites, which is surface intensified and reverses in the deep layer with a zero-crossing depth range from 1500 m to 1800 m as latitude increases. However, using this single mode will largely underestimate the full velocity. The barotropic mode is depth independent, strengthening the upper layer flow and weakening the deep layer flow. Moreover, the EOF1 also drops from the surface to the deep ocean but does not reverse, which contains a mixed signal of barotropic and first baroclinic modes. Therefore, it is reasonable to assume that the barotropic and first baroclinic modes tend to cancel each other at the bottom, and we could linearly sum up these two modes. The

projection coefficients of the summed vertical mode and the PC1 are nearly identical. Since the vertical profiles of the dominant vertical mode from the two methods (EOF1 and $C_s(z)$) are normalized to 1 at the surface, the projection coefficients (PC1 and $P_s(t)$) could be approximated by the surface geostrophic current flow.

Therefore, we found a remarkable relationship that connects the surface geostrophic current and the vertical structure of the zonal current in the KE region. This relationship is tested extensively for the whole KE region by using the OFES datasets, which shows that this relationship could hold in the whole KE region. Then we use this method to estimate the KE transport and compare it with some historical sections. The estimated KE transport is generally in agreement with the observations along the 147°E line and the KESS observation (Jayne et al., 2009). These results show that the mode estimation method could well reproduce the KE transport. This method provides a more direct estimation of the KE and its vertical structure, which can be calculated using AVISO geostrophic flow and WOA hydrographic data. Furthermore, the KE transport is easy to be estimated based on the vertical structure, which is an essential basis for studying the climate influences of the KE.

It should be noted that the projection coefficient is weaker than the surface geostrophic current for some strong currents. A detailed check shows that the vertical structure will be affected by non-local eddies. These eddies will bring seawater with different hydrographic information, which contaminates the local vertical structure. This feature will be improved by using time-dependent T/S data in OFES. However, even in the OFES, there are still some peaks where the geostrophic current is stronger than the mode projection coefficient. This is because we have not taken centrifugal force or non-linear terms into consideration, which will break the geostrophic balance, especially for strong eddies. Nevertheless, this mode estimation method could well reproduce the main structure and over 80% variance of the KE transport.

Acknowledgments

This research is financially supported by the National Natural Science Foundation of China (42225601, 42076009, 42176006), and Fundamental Research Funds for the Central Universities (202072001, 202241006). Z. Chen is partly supported by the Taishan Scholar Funds (tsqn201812022).

Data Availability Statement

The mooring data are available at the Kuroshio Extension Mooring System website (https://cn-kems.net/Data/data.zip.001; https://cn-kems.net/Data/data.zip.002). The AVISO data are available at https://sso.altimetry.fr/. The World WOA 18 data are available at https://www.ncei.noaa.gov/archive/accession/NCEI-WOA18. The OFES data are downloaded from University of Hawaii website https://apdrc.soest.hawaii.edu/datadoc/ofes/ofes.php. Hydrographic data from and 147°E section is downloaded from Japan Meteorological Agency website http://www.data.jma.go.jp/gmd/kaiyou/db/vessel_obs/data-report/html/ship/ship.php.

References

Bishop, S. P., Watts, D. R., Park, J. H., & Hogg G., N. G. (2012). Evidence of bottom-trapped currents in the Kuroshio Extension region. *Journal of Physical Oceanography*, *42*(2), 321–328. doi:10.1175/JPO-D-11-0144.1

Ducet, N., Le Traon, P. Y., & Reverdin, G. (2000). Global high-resolution mapping of ocean circulation from TOPEX/Poseidon and ERS-1 and -2. *Journal of Geophysical Research: Oceans*, *105*(C8), 19477–19498. doi:10.1029/2000jc900063

Hall, M. M. (1989). Velocity and transport structure of the Kuroshio Extension at 35°N, 152°E. *Journal of Geophysical Research*, *94*(C10), 14445. doi:10.1029/JC094iC10p14445

Hiroe, Y., Yasuda, I., Komatsu, K., Kawasaki, K., Joyce, T. M., & Bahr, F. (2002). Transport of North Pacific intermediate water in the Kuroshio-Oyashio interfrontal zone. *Deep-Sea Research Part II: Topical Studies in Oceanography*, *49*(24–25), 5353–5364. doi:10.1016/S0967-0645(02)00195-9

Hurlburt, H. E., Wallcraft, A. J., Schmitz, W. J., Hogan, P. J., & Metzger, E. J. (1996). Dynamics of the Kuroshio/Oyashio current system using eddy-resolving models of the North Pacific Ocean. *Journal of Geophysical Research: Oceans*, *101*(C1), 941–976. doi:10.1029/95JC01674

Jayne, S. R., Hogg, N. G., Waterman, S. N., Rainville, L., Donohue, K. A., Randolph Watts, D., et al. (2009). The Kuroshio Extension and its recirculation gyres. *Deep Sea Research Part I: Oceanographic Research Papers*, *56*(12), 2088–2099. doi:10.1016/j.dsr.2009.08.006

Joyce, T. M. (1987). Hydrographic sections across the Kuroshio extension at 165°E and 175°W. *Deep Sea Research Part A, Oceanographic Research Papers*, *34*(8), 1331–1352. doi:10.1016/0198-0149(87)90130-0

Kalnay, E., Kanamitsu, M., Kistler, R., Collins, W., Deaven, D., Gandin, L., et al. (1996). The NCEP/NCAR 40-Year Reanalysis Project. *Bulletin of the American Meteorological Society*, *77*(3), 437–471. doi:10.1175/1520-0477(1996)077<0437:TNYRP>2.0.CO;2

Kida, S., Mitsudera, H., Aoki, S., Guo, X., Ito, S. ichi, Kobashi, F., et al. (2015). Oceanic fronts and jets around Japan: a review. *Journal of Oceanography*, *71*(5), 469–497. doi:10.1007/s10872-015-0283-7

Locarnini, R. A., Mishonov, A. V., Baranova, O. K., Boyer, T. P., Zweng, M. M., Garcia, H. E., et al. (2019). World Ocean Atlas 2018, Volume 1: Temperature. A. Mishonov, Technical Editor. *NOAA Atlas NESDIS*, *81*(July), 52.

Long, Y., Zhu, X. H., & Guo, X. (2019). The Oyashio Nutrient Stream and Its Nutrient Transport to the Mixed Water Region. *Geophysical Research Letters*, *46*(3), 1513–1520. doi:10.1029/2018GL081497

Long, Y., Zhu, X. H., Guo, X., & Huang, H. (2018). Temporal Variation of Kuroshio Nutrient Stream South of Japan. *Journal of Geophysical Research: Oceans*, *123*(11), 7896–7913. doi:10.1029/2017JC013635

Ma, X., Jing, Z., Chang, P., Liu, X., Montuoro, R., Small, R. J., et al. (2016). Western boundary currents regulated by interaction between ocean eddies and the atmosphere. *Nature*, *535*(7613), 533–537. doi:10.1038/nature18640

Ma, J., Hu, S., Hu, D., Villanoy, C., Wang, Q., Lu, X., & Yuan, X. (2022). Structure and Variability of the Kuroshio and Luzon Undercurrent Observed by a Mooring Array. *Journal of Geophysical Research: Oceans*, *127*(2), 1–12. doi:10.1029/2021jc017754

524 Masumoto, Y., Sasaki, H., Kagimoto, T., Komori, N., Ishida, A., Sasai, Y., et al. (2004). A Fifty-
525 Year Eddy-Resolving Simulation of the World Ocean - Preliminary Outcomes of OFES (OGCM
526 for the Earth Simulator). *Journal of the Earth Simulator*, *1*, 35–56.
527 Oliver, E. C. J., Benthuysen, J. A., Darmaraki, S., Donat, M. G., Hobday, A. J., Holbrook, N. J.,
528 et al. (2021). Marine Heatwaves. *Annual Review of Marine Science*, *13*, 313–342.
529 doi:10.1146/annurev-marine-032720-095144
530 Qiu, B. (2003). Kuroshio extension variability and forcing of the Pacific decadal oscillations:
531 Responses and potential feedback. *Journal of Physical Oceanography*, *33*(12), 2465–2482.
532 doi:10.1175/2459.1
533 Qiu, B., Chen, S., & Hacker, P. (2007). Effect of mesoscale eddies on subtropical mode water
534 variability from the Kuroshio Extension System Study (KESS). *Journal of Physical*
535 *Oceanography*, *37*(4), 982–1000. doi:10.1175/JPO3097.1
536 Ren, Q., Li, Y., Wang, F., Song, L., Liu, C., & Zhai, F. (2018). Seasonality of the Mindanao
537 Current/Undercurrent System. *Journal of Geophysical Research: Oceans*, *123*(2), 1105–1122.
538 doi:10.1002/2017JC013474
539 Suga, T., & Hanawa, K. (1995). The Subtropical Mode Water Circulation in the North Pacific.
540 *Journal of Physical Oceanography*, *25*(5), 958–970. doi:10.1175/1520-
541 0485(1995)025<0958:TSMWCI>2.0.CO;2
542 Talley, L. D., Nagata, Y., Fujimura, M., Iwao, T., Kono, T., Inagake, D., et al. (1995). North
543 Pacific Intermediate Water in the Kuroshio/Oyashio Mixed Water Region. *Journal of Physical*
544 *Oceanography*, *25*(4), 475–501. doi:10.1175/1520-0485(1995)025<0475:NPIWIT>2.0.CO;2

Tsunogai, S., Ono, T., & Watanabe, S. (1993). Increase in total carbonate in the western North Pacific water and a hypothesis on the missing sink of anthropogenic carbon. *Journal of Oceanography*, *49*(3), 305–315. doi:10.1007/BF02269568

Vallis, G. K. (2017). *Atmospheric and oceanic fluid dynamics*. Cambridge University Press.

Yang, Y., Liang, X. S., & Sasaki, H. (2021). Vertical coupling and dynamical source for the intraseasonal variability in the deep Kuroshio Extension. *Ocean Dynamics*, *71*(11–12), 1069–1086. doi:10.1007/s10236-021-01482-9

Yasuda, I. (2004). North Pacific intermediate water: Progress in SAGE (SubArctic Gyre Experiment) and related projects. *Journal of Oceanography*, *60*(2), 385–395. doi:10.1023/B:JOCE.0000038344.25081.42

Yoshikawa, Y., Church, J. A., Uchida, H., & White, N. J. (2004). Near bottom currents and their relation to the transport in the Kuroshio Extension. *Geophysical Research Letters*, *31*(16), 1–5. doi:10.1029/2004GL020068

Zhu, R., Chen, Z., Zhang, Z., Yang, H., & Wu, L. (2020). Subthermocline Eddies in the Kuroshio Extension Region Observed by Mooring Arrays. *Journal of Physical Oceanography*, *51*(2), 439–455. doi:10.1175/jpo-d-20-0047.1

Zweng, M. M., Reagan, J. R., Seidov, D., Boyer, T. P., Antonov, J. I., Locarnini, R. A., et al. (2019). World Ocean Atlas 2018 Volume 2: Salinity. *NOAA Atlas NESDIS*, *82*(July), 50pp. Retrieved from http://www.ncei.noaa.gov/sites/default/files/2020-04/woa18_vol2.pdf